Luo, Y., Acosta, A.R., Austin, J.M., Hornung, H.G.: Co-linear Focused Laser Differential Interferometry and Schlieren Measurements of Supersonic Cylinder Near Wake. California Institute of Technology, Pasadena, CA, USA. Presented at the 35th International Symposium on Shock Waves (ISSW35), Brisbane, Australia, 05-14 July 2025.

Co-linear Focused Laser Differential Interferometry and Schlieren Measurements of Supersonic Cylinder Near Wake

Ying Luo, Alex R. Acosta, Joanna M. Austin, and Hans G. Hornung

California Institute of Technology, Pasadena, CA, 91125, USA
yluo3@caltech.edu

Abstract. Co-linear focused laser differential interferometry (FLDI) with simultaneous beam tracking in high-speed schlieren (HSS) was developed to investigate the near wake of a cylinder in Mach 4 flow. Validation of the combined system was performed using an accelerometer and linear displacement sensor, with a vibrating cylindrical lens as the phase object. Using this colinear diagnostic, two frequencies were found to be associated with the shear layer. The most dominant frequency observed confirmed both the frequency values and the Strouhal number independence from Re_D when scaled by shear layer length, as previously reported by Schmidt and Shepherd [1]. Additionally, it was shown that the same frequency persists along the latter half of the shear layer. A broader and lower-amplitude peak was also observed at 7–8 kHz across all conditions, unchanging with Re_D. The origin of this secondary frequency is unclear, and under further investigation.

Keywords: fldi, schlieren, cylinder, wake dynamics, supersonic wake

1 Introduction

The flow over a cylinder is a classical canonical problem studied extensively in the low-speed incompressible flow regime, where across a range of Reynolds numbers, the unsteadiness in the wake is characterised by vortex shedding from the cylinder surface. In comparison, experimental studies of cylinder wakes in the high-speed compressible regime are limited. Recently, using time-resolved shadowgraph, Schmidt and Shepherd [1] found that a cylinder in Mach 4 flow exhibits temporal periodicity in the near-wake region at a higher frequency than its incompressible counterpart. As the authors note, the mechanisms for the oscillations in the two flow regimes are likely to differ. Defining the Strouhal number as the distance from the separation points to the neck, Schmidt and Shepherd [1] found universal collapse for the Reynolds numbers studied, indicating the oscillations are sustained by communication between the neck and separation points along the shear layer through the subsonic region. Thasu and Duvvuri [2] provided evidence of this using pressure measurements on the cylinder surface. Recently, using insights from cavity flows, Thasu et al.[4] has progressed

this theory further and developed an analytical aeroacoustic model based on a feedback loop between vortical disturbances propagating through the shear layer and upstream propagation of acoustic waves in the subsonic region of the shear layer. Model predictions are in good agreement with experimentally observed frequencies. Awasthi et al. [3] experimentally observed standing waves in the wake, attributed to interference between downstream-propagating instabilities and upstream-propagating acoustic waves. It was hypothesised that the upstream waves originate from unsteady shear layer separation on the cylinder since they appear upstream of the compression region. These waves travel through the supersonic flow until they reach the subsonic portion of the early wake, where they can interact with the downstream propagating instabilities to form standing waves.

In order to further study the near wake of a cylinder in supersonic flow, co-linear focused differential interferometry (FLDI) and high-speed schlieren (HSS) was developed. Simultaneous HSS and FLDI was first used successfully to measure freestream density fluctuations with FLDI and pitot probe shock standoff distance with HSS by Bathel et al. [5]. Thus, the objective of this current work is to validate the co-linear HSS and FLDI diagnostic, corroborate shadowgraph measurements made by Schmidt and Shepherd [1] using the developed diagnostic, provide further data by probing different regions of the shear layer, and contribute to the understanding of unsteady flow characteristics in the near-wake region of a supersonic cylinder.

2 Experimental Setup

2.1 Facility & Model

The experiments in this paper were conducted in the Caltech Ludwieg Tube using air as the test gas. The facility consists of a 17-meter-long driver tube with an inner diameter of 300 mm, pressurised to the desired driver pressure (P_{driver}). Upon opening the piston valve, the high-pressure gas in the driver tube expands through an axisymmetric converging-diverging nozzle, generating a steady Mach 4 test flow for approximately 60 - 80 ms. A more detailed description of the facility is found in Mouton [6]. The nominal freestream flow conditions used for this experiment are summarised in Table 1. The model used in this experiment is a precision-ground aluminium cylinder with a diameter of 19.05 mm. Both the cylinder and the mount are the same as those used in Schmidt and Shepherd [1].

2.2 Co-linear FLDI and HSS

The primary diagnostic techniques developed and used to investigate the cylinder near wake is co-linear FLDI and HSS. This enables simultaneous, time-synced off-body spatial gradient of density measurements and flow visualization.

This FLDI system is based on the work of Lawson [7]. It uses the Hübner Photonics Cobolt 05-01 Samba laser at $\lambda = 532$ nm. The laser is expanded

Table 1: Freestream Conditions.

P_{driver} (kPa)	M_∞	P_∞ (kPa)	u_∞ (m/s)	T_∞ (K)	ρ_∞ (kg/m^3)	Re_D
150	4	0.92	667	69	0.046	1.18×10^5
200	4	1.23	667	69	0.063	1.58×10^5
250	4	1.53	667	69	0.067	1.96×10^5
350	4	2.14	667	69	0.108	2.76×10^5

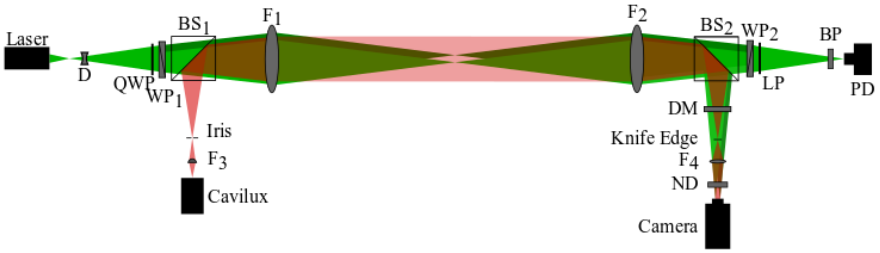

Fig. 1: Schematic of the co-linear single point FLDI system and HSS system.

using a plano concave lens (f = -9 mm) (**D**) before being circularly polarised using a quarter wave plate (**QWP**). A Wollaston prism (**WP**$_{1,2}$) with a two arc-minute separation is used to split the beams, which are then passed through a 75 mm diameter plano-convex lens (f = 250 mm) (**F**$_{1,2}$) which focuses the beams onto the model. The catch side is symmetric, with the exception that a linear polariser (**LP**) is used instead of a quarter wave plate. The beams are focused onto a Thorlabs PDA36A2 photodetector (**PD**), and the signal is sampled at 1 MHz. The final beam spacing is 145 $\pm 2\mu m$ with a beam diameter of 10.5 $\pm 2\mu m$.

The HSS portion of the diagnostic uses the Cavilux HF (λ = 640 nm) pulsed at 64020 Hz with a pulse width of 30 ns. The light is focused using an aspheric lens (f = 15mm) (**F**$_3$). The schlieren light is introduced into the FLDI system using 2" cube non-polarising 50:50 beam splitters (**BS**) placed between **F**$_{1,2}$ and **WP**$_{1,2}$. The use of a cube beam splitter eliminates the refractive index offset compensation required with a dichroic mirror. Both HSS and FLDI systems use **F**$_{1,2}$ as their focusing component. On the catch side, a beamsplitter redirects the schlieren light through a λ = 550 nm long pass dichroic mirror, a knife-edge, a neutral density filter (OD: 0.5) (**ND**), a focusing lens (f = 250 mm) (**F**$_4$), and into the Phantom v1612 high-speed camera run at 64020 Hz, with a resolution of 640 x 336 pixels. A schematic of the optical setup is provided in Fig. 1.

The post-processing of the FLDI signals follows a similar methodology to Lawson [7]. The frequency domain results are presented as a power spectral density (PSD) of the estimated denoised FLDI phase response $\Delta\phi(t)$. The schlieren is transformed from a lab-stationary frame to a model-stationary frame by re-

moving facility structural vibrations/movement. The results are also presented as a PSD, obtained by sampling the pixel intensity at specific locations.

2.3 FLDI Response Validation

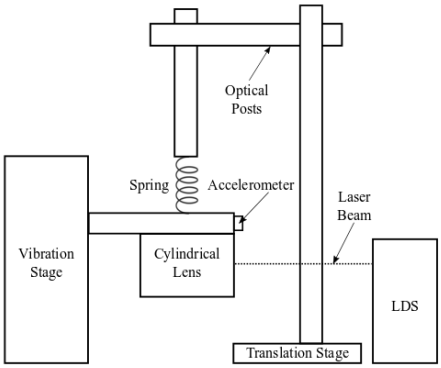

Fig. 2: Schematic of the FLDI validation setup.

A validation test for the two systems was performed by adapting an approach developed by Hameed [8]. The response of the FLDI system was tested using a converging cylindrical lens (f = 500 mm) as the phase object. A schematic of the setup is shown in Fig. 2. The cylindrical lens was suspended by a compliant spring attached to an optical post mounted to translation stages for precise positioning along and perpendicular to the optical path. The lens was driven at a prescribed frequency using a function generator (Stanford Systems DS335) and a vibration driver (3B Scientific 1000701), with the lens centered at the FLDI beam focus. A linear displacement sensor (LDS) (Keyence LK-GD500) and accelerometer (PCB352A21) measured the motion of the lens to validate FLDI amplitude and frequency response. This setup models a sinusoidal density disturbance field normal to the optical path and is assumed to be infinitesimally thin along the optical path.

The phase change from the raw FLDI signal can be determined via [7]

$$\Delta\phi = sin^{-1}\left(\frac{V-D}{A}\right) + \Delta\phi_0, \tag{1}$$

where $A = (V_{max} - V_{min})/2$, $D = (V_{max} + V_{min})/2$, and $\Delta\phi_0$ is when $\Delta\phi = 0$.

The phase difference between the FLDI beam pairs due to the distinct optical paths can be derived geometrically and has the following form:

$$\Delta\phi = \frac{2\pi}{\lambda}\left[(n_g - n_a)\left(\sqrt{R^2 - (\Delta x/2 - x)^2} - \sqrt{R^2 - (\Delta x/2 + x)^2}\right)\right], \tag{2}$$

where n_g and n_a are the refractive indices of the glass and ambient environment, respectively, R is the radius of curvature of the cylindrical lens, Δx is the distance between the two FLDI beams, and x is the displacement from the origin. A detailed derivation of Eqn. 2 can be found in Hameed [8]. The phase response of the LDS and accelerometer can be found using the Eqn. 2.

The cylindrical lens was forced at a number of frequencies from 25 to 300 Hz; the results for 30 Hz presented in Fig. 3 are representative. The phase change between all three measurements agrees reasonably well with each other, with a maximum phase difference of 0.1608 and 0.0689 radians between the accelerometer and FLDI, and FLDI and LDS, respectively. Similarly, in the frequency space, all measurements have excellent agreement at the fundamental frequency and a few harmonics. The results from the accelerometer show greater deviation from the other two measurements, likely due to an unideal mounting location and/or attachment method. Despite this, this setup has proved that the additional HSS optics do not affect the FLDI response.

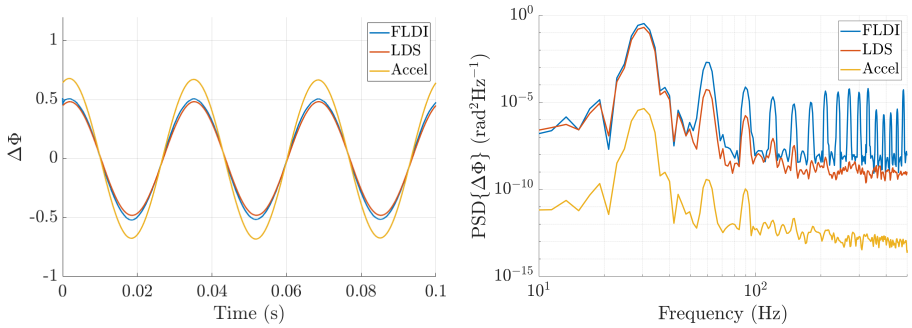

Fig. 3: Phase change measured (left) and PSD of the phase change response (right) from FLDI, LDS, and accelerometer through the cylindrical lens.

3 Results and Discussion

A representative schlieren image is shown in Fig. 4 to demonstrate the mean flow structure behind a cylinder at $Re_D = 2.76\times10^5$ and Mach 4. The flow features seen in this image are representative of all other conditions. Behind the cylinder, the flow turns through a series of expansion waves, forming a separation shear layer and separation shock. The shear layers converge downstream to a finite-width neck. The turbulent wake is formed through a series of compression waves that coalesce to form a recompression shock. Importantly, the locations of the FLDI points are detected in the HSS images.

The PSDs of the estimated denoised FLDI phase response $\Delta\phi(t)$ for $Re_D = 1.96\times10^5$ and $Re_D = 2.76\times10^5$ at three locations along the shear layer (FLDI beam position for repeat experiments are marked on the schlieren) are presented

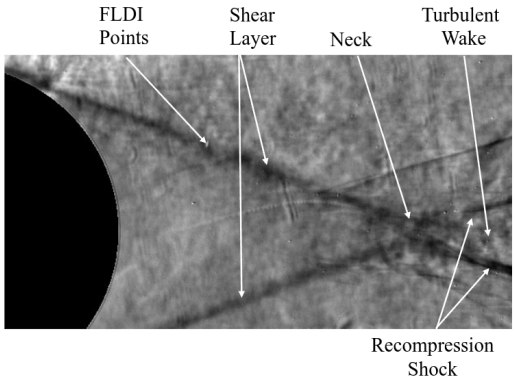

Fig. 4: Schlieren image at $Re_D = 2.76\times10^5$ to illustrate mean flow.

in Figs. 5 and 6, respectively. For both conditions, it can be observed that the peak at around 16.1 kHz and 16.7 kHz for $Re_D = 1.96\times10^5$ and $Re_D = 2.76\times10^5$, respectively, is strongest near the neck. The PSD of the point closest to the neck has more energy than the other two locations since it is closer to the wake. By using the same cylinder diameter and similar flow conditions as Schmidt and Shepherd [1], we have been able to experimentally measure the same frequency observed by Schmidt and Shepherd [1] using FLDI.

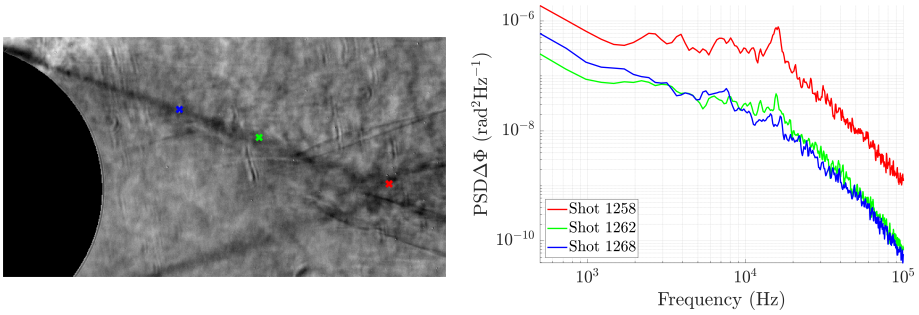

Fig. 5: Schlieren overlayed with probed FLDI positions (left) and the PSD of the FLDI phase response in the shear layer (right) at $Re_D = 1.96\times10^5$.

This high-frequency peak associated with the shear layer oscillation identified by the FLDI can also be extracted from the simultaneous HSS. Fig. 7 presents the average PSD of 15 pixels perpendicular to the shear layer at three locations along the shear layer. The 15 pixel averaging is employed to provide improved statistical averaging. From the schlieren, the peak is around 15.8 kHz and 16.5 kHz for the $Re_D = 1.96\times10^5$ and $Re_D = 2.76\times10^5$, respectively.

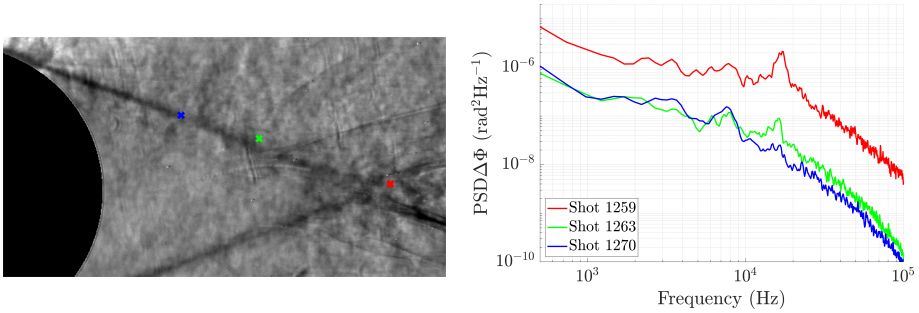

Fig. 6: Schlieren overlayed with probed FLDI positions (left) and the PSD of the FLDI phase response in the shear layer (right) at $Re_D = 2.76\times10^5$.

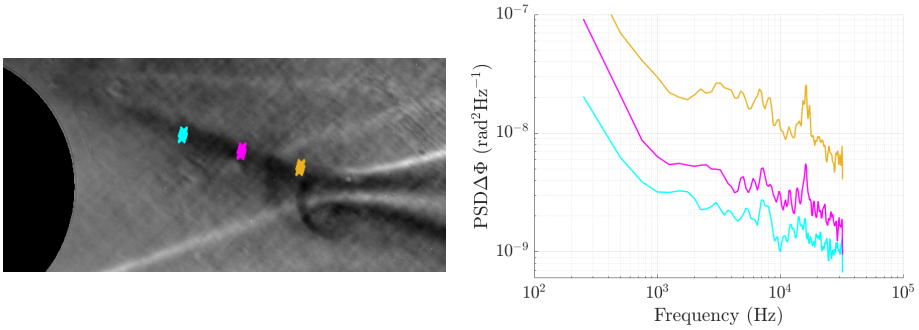

Fig. 7: Average spectra of pixels perpendicular to the shear layer at 3 locations along the shear layer.

In both FLDI and schlieren measurements across all conditions, the high-frequency peak appears not only near the neck but also further upstream within the shear layer, with no change in frequency observed along the probed locations. However, the peak does decrease in magnitude until it is barely discernible around halfway along the shear layer. Given that Thasu and Duvvuri [2] were able to detect the same oscillatory frequency at the separation point using pressure transducers, this suggests that the high frequency peak is likely present throughout the shear layer, and it is due to the limitations of the FLDI/schlieren diagnostic that the peak cannot be detected. This further supports the model proposed by Thasu et. al. [4], in which shear layer oscillations are driven by an aeroacoustic feedback loop where vortical disturbances propagating through the shear layer interact with upstream propagation of acoustic waves generated at the neck from shear layer interactions. Table 2 tabulates the observed shear layer oscillation frequencies for all the conditions; the two values agree to within 0.5 kHz.

In addition to the strong high-frequency peak at $\sim 13.5 - 16.7$ kHz, associated with the shear layer oscillation, a secondary, lower amplitude and more

Table 2: Shear layer oscillation frequency obtained from schlieren and FLDI in the neck region in the cylinder near wake.

P_{driver} (kPa)	Re_D	Schlieren (kHz)	FLDI (kHz)
150	1.18×10^5	13.5	13.7
200	1.58×10^5	15	14.5
250	1.96×10^5	15.8	16.1
350	2.76×10^5	16.5	16.7

broadband peak at $\sim 7 - 8$ kHz is also observed in both the FLDI and HSS results. Given the broadband and low-amplitude nature, a precise frequency is more difficult to extract. This low-frequency peak, however, does appear in all conditions at $\sim 7 - 8$ kHz. From Fig. 5 and 6, it is most notable in the FLDI points closest to the separation point. This might be a subharmonic of the shear layer frequency or indicative of another instability present within the flow.

Examining the coherence between pixels within the shear layer and the wake, Awasthi [3] detected a weak localised ridge in the coherence map, indicating a secondary lower frequency within the shear layer and the early wake. This feature was hypothesised to arise from a Kelvin–Helmholtz (KH) instability, which may grow before rapidly decaying, as compressibility stabilises the KH instability. We see a similar trend in the FLDI data for each condition, where the peak decreases in magnitude as we move downstream. However, the change in Re_D for each condition should produce differences in the observed frequency. While it is possible that the frequency is indeed changing with each condition, the broad and noisy nature of the peak limits the ability to discern this change. Further analysis is required to provide a definitive answer.

To compare the consistency of the spectral estimates from HSS and FLDI, we plot the premultipled normalised spectra obtained from a point just upstream of the neck in Fig. 8. It can be seen that the spectra are very similar between the two measurements, indicating that both systems capture the same dominant flow features. There is also a similar distribution of energy across frequency bands, particularly the two dominant frequencies, where the width and height of the peaks are almost identical. We note that the spectra from the schlieren are obtained by averaging over many pixels, since the signal from any individual pixel is extremely weak. Therefore, it is not a true point measurement, and this loss of spatial specificity introduces some interpretational ambiguity. Additionally, the schlieren measurements exhibit a higher noise floor at high frequencies compared to FLDI ($>\sim 20$ kHz in this case) and are more limited in the available sampling frequency. These limitations demonstrate the utility of simultaneous measurements of a particular flow field. The schlieren is able to provide entire flow field visualization, precise FLDI beam positions, and confirmatory frequency analysis, whilst the FLDI yields improved frequency and quantitative density gradient information.

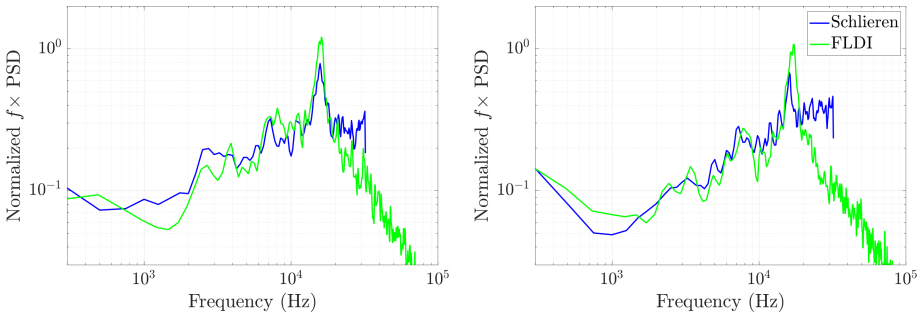

Fig. 8: Premultiplied normalised spectra of the FLDI and schlieren for the conditions $Re_D = 1.96\times10^5$ (left) and $Re_D = 2.76\times10^5$ (right).

To compare the results from this study with those from Schmidt [1], the Strouhal number of the shear layer oscillation frequency scaled by diameter (St_D) and shear layer length (St_S) is plotted against Re_D in Fig. 9. The uncertainty in St_D and St_S is based on the estimates of the full-width at half-maximum of the frequency peak in the spectra. The St_D scaling agrees with the data obtained by Schmidt and Shepherd [1] and follows the power-law dependence between St_D and Re_D observed in incompressible flow. Similarly, St_S does not exhibit any dependence on the Re_D and has an average value of 0.566 for FLDI and 0.564 for schlieren. The spread of the St_S values across the tested Re_D is narrower than the results reported by Schmidt and Shepherd [1], yielding an average value slightly higher than their value of 0.48. However, all the data fall within the error bars of experimental variation and uncertainty. Nonetheless, the data obtained from the FLDI conforms to the trends observed by Schmidt and Shepherd [1] and corroborates St_S universality with respect to Reynolds number.

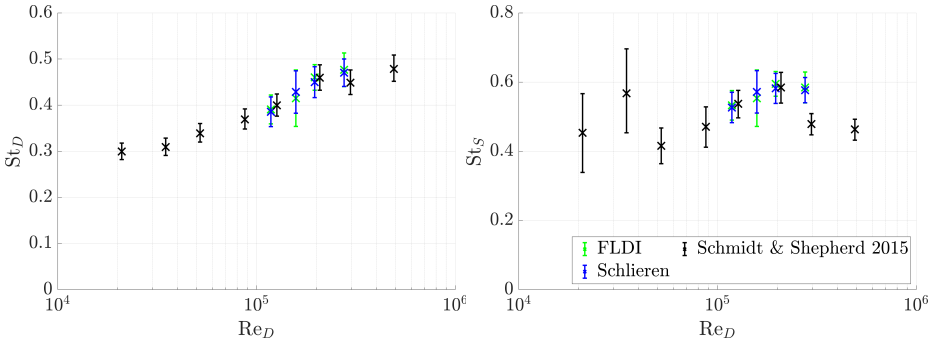

Fig. 9: Variation of Strouhal number based on cylinder diameter (left) and shear layer length (right) with Reynolds number.

4 Conclusion

Co-linear focused laser differential interferometry and schlieren measurements were made of the cylinder near wake in Mach 4 flow at four Re_D. Premultiplied and normalised spectra from both FLDI and HSS were consistent, corroborating that each technique captures the same dominant flow feature—namely, the shear layer. Two main frequencies were identified in the spectra. The most prominent high-frequency peak, linked to oscillations of the shear layer, experimentally confirmed values previously reported by Schmidt and Shepherd [1]. It was also shown via HSS and FLDI that this frequency persisted along the latter half of the shear layer. In agreement with Schmidt and Shepherd [1], scaling the measured frequency by the shear layer length yields a Strouhal number, St_S, independent of Re_D with a value of 0.566 for FLDI and 0.564 for schlieren. A second frequency peak, broader and lower in magnitude, is also found. However, unlike the higher frequency peak, it does not seem to vary across the different conditions, remaining at around 7-8 kHz. The origin of this secondary frequency remains unclear, and further experiments and analysis are necessary to achieve a comprehensive understanding of the wake dynamics behind the cylinder.

5 Acknowledgments

This work was partially supported by the Air Force Office of Scientific Research under Award No. FA9550-23-1-0446, with Dr. Amanda Chou as program officer.

References

1. Schmidt, B.E., Shepherd, J.E.: Oscillations in cylinder wakes at Mach 4. J. Fluid Mech. 785, R3 (2015). doi:10.1017/jfm.2015.628
2. Thasu, P.S., Duvvuri, S.: Strouhal number universality in high-speed cylinder wake flows. Phys. Rev. Fluids 7, L081401 (2022). doi:10.1103/PhysRevFluids.7.L081401
3. Awasthi, M., McCreton, S., Moreau, D.J., Doolan, C.J.: Supersonic cylinder wake dynamics. J. Fluid Mech. 945, A2 (2022). doi:10.1017/jfm.2022.624
4. Thasu, P.S., Kumar, G., Duvvuri, S.: Aeroacoustic mechanisms explain universal behaviour in high-Mach number cylinder wakes. J. Fluid Mech. 1010 (2025). doi: 10.1017/jfm.2025.305
5. Bathel, B.F., Herring, G.C., Weisberger, J.M., Chou, A., Jones, S.B.: Simultaneous focused laser differential interferometry and high-speed schlieren in a Mach 6 flow. Meas. Sci. Technol. 32, 095907 (2021). doi:10.1088/1361-6501/abfef5
6. Mouton, C.A.: Transition Between Regular Reflection and Mach Reflection in the Dual-Solution Domain. Ph.D. thesis, California Institute of Technology (2007). doi:10.7907/TEA0-Q468
7. Lawson, J.M.: Focused Laser Differential Interferometry. Ph.D. thesis, California Institute of Technology (2021). doi:10.7907/5thh-f652
8. Hameed, A.: Spectral Analysis of Hypersonic Boundary-Layer Instability. Ph.D. thesis, Stevens Institute of Technology (2023).